JOURNAL OF COMPUTATIONAL PHYSICS 10, 107–122 (1972)

An Application of the Shooting Method to the Stability Problem for a Stratified, Rotating Boundary Layer

R. A. BROWN

Advanced Study Program, National Center for Atmospheric Research, Boulder, Colorado*

AND

F. LEE

Department of Oceanography, University of Washington, Seattle, Washington 98105

Received October 25, 1971

I. INTRODUCTION

The stability analysis for a stratified fluid in a rotating coordinate system results in an eighth-order eigenvalue equation. For various limiting conditions, this equation can be reduced to a sixth-, fourth- or second-order eigenvalue equation. In particular, the fourth-order approximation for neutral stratification is the Orr–Sommerfeld (O–S) equation. The stratified Orr–Sommerfeld equation has been investigated numerically for convective instability and Couette flow (linear velocity profile) [1], and for Couette, Poiseuille (parabolic velocity profile) and an arbitrary velocity profile with an inflection point [2]. The mean flow considered here is the geophysical boundary layer solution for a balance between Coriolis and viscous forces. This solution yields a spiral velocity profile from the surface to the free stream velocity. The velocity profile confronted by the two-dimensional perturbation will depend upon the orientation, here defined as the angle to the left of the free stream velocity. These velocity profiles are shown in Fig. (1). Note that the velocity profiles exhibit a "strong" inflection point, since there is a large velocity gradient at the inflection point. This results in a well defined instability mode at low wavenumbers.

The equations with these velocity profiles as parameters have been solved by finite differencing [3] and using the shooting method [4] with similar results. The relative merits of the two methods has been discussed by Gary and Helgason [5]

* The National Center for Atmospheric Research is sponsored by the National Science Foundation.

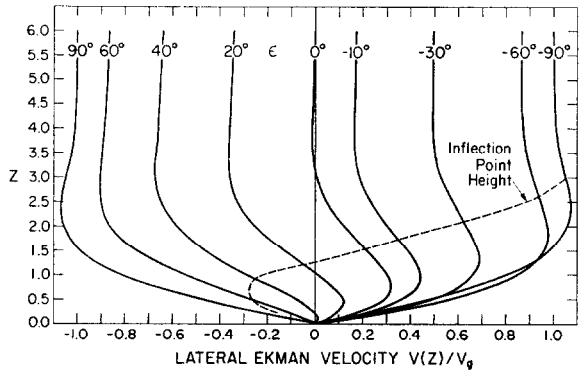

FIG. 1. Velocity profiles from a viscous-Coriolis force balance (Ekman layer) in a vertical plane at an angle $\epsilon + 90°$ to the left of the geostrophic (free stream) velocity V_g (Northern hemisphere).

with emphasis on the matrix method employing the Q–R algorithm. In this paper we discuss the shooting method as applied to the second-, fourth- and sixth-order equations.

The shooting method with a purification scheme as we have used requires a single, n-th-order differential equation. Assuming n boundary conditions at one boundary (generally complete smoothness at infinity), an eigenvalue can be guessed, the equation integrated, and the difference at the other boundary condition evaluated as a function of the eigenvalue. The roots of this functional relationship then define solution eigenfunctions which satisfy both boundary conditions.

The conservation equations for a geophysical fluid in a rotating system produce the following set of equations when subjected to a two-dimensional simple harmonic perturbation; coordinate alignment such that $\partial/\partial x = 0$; linearization and non-dimensionalization with respect to $L = (K_m/\Omega \sin\theta)^{1/2}$, V_g and $t = L/V_g$. K_m is the eddy viscosity, Ω is the vertical component of the system rotation, V_g is the geostrophic, or free stream velocity, and θ is the latitude.

$$\begin{aligned} u_t + Vu_y - \psi_y V_z - 2E\psi_z - E\,\nabla^2 u &= 0, \\ \psi_{zt} + V\psi_{zy} - \psi_y V_z + 2Eu - E\,\nabla^2\psi_z + p_y &= 0, \\ \psi_{yt} + V\psi_{yy} - g_0 T/\bar{T} - E\,\nabla^2\psi_y - p_z &= 0, \\ T_t + VT_y - \psi_y(\bar{T}_z + \Gamma) - (E/Pr)\,\nabla^2 T &= 0, \end{aligned} \tag{1}$$

where

$$v = \psi_z\,, \qquad w = -\psi_y \qquad \psi = \text{stream function}$$

$$E = (2K_m\Omega \sin\theta)^{1/2}/2V_g\,, \qquad \Gamma = (g/c_p)(L/T), \qquad Pr = K_m/K_n\,.$$

Here, E represents either the inverse of the Reynolds number or the Rossby number as they are not independent for a semi-infinite fluid.

We introduce periodic solutions for u, ψ and T, and eliminate p by cross differentiation,

$$\begin{Bmatrix} \psi \\ u \\ T \end{Bmatrix} = \begin{Bmatrix} \phi \\ \mu \\ \tau \end{Bmatrix} e^{i\alpha(y-ct)}$$

$$\begin{aligned}
(V-c)\,\mu - V'\phi - \frac{E}{i\alpha}(\mu'' - \alpha^2\mu) - \frac{2E}{i\alpha}\phi' &= 0 \\
(V-c)\,\tau - S\overline{T}\phi - \frac{E}{i\alpha Pr}(\tau'' - \alpha^2\tau) &= 0 \\
(V-c)\,\phi'' - [V'' + \alpha^2(V-c)]\,\phi & \\
- \frac{E}{i\alpha}(\phi'''' - 2\alpha^2\phi'' + \alpha^4\phi) + \frac{2E}{i\alpha}\mu' + \frac{g_0}{\overline{T}}\tau &= 0 \\
S \equiv \frac{1}{\overline{T}}(\overline{T}_z + \Gamma), \qquad &\text{the stability,} \quad \phi' \equiv \partial/\partial z.
\end{aligned} \tag{2}$$

While it does not appear to be possible to obtain a single equation in ϕ as the dependent variable, an eighth-order equation in τ can be written in operator form. However, the expansion to coefficient form is cumbersome, and the chance of error is great. These considerations, in addition to the long computational times anticipated for the eighth-order integration, led to the investigation of the problem for limiting cases, hoping that the complete stability problem could be inferred from the stability solutions of the lower-order equations obtained when different terms in the basic set were neglected. Thus, a second-order equation is obtained by neglecting viscous and Coriolis forces, a fourth-order equation by neglecting Coriolis and stratification terms, and a sixth-order equation by neglecting the Coriolis terms only. The sixth-order set with the Ekman profile as a parameter and neglecting stratification terms was solved in [3].

The following eigenvalue equations with coefficients variable in $V(z)$, Ri, α, E and Pr are to be solved for eigenvalues c and eigenfunctions ϕ. We are particularly interested in the maximum growth rate, $(\alpha c_i)_{\max}$.

$$\left\{D^2 - \alpha^2 - \frac{V''}{V-c} + \frac{Ri}{(V-c)^2}\right\}\phi = 0, \tag{3}$$

$$\left\{(V-c)(D^2-\alpha^2) - V'' - \frac{E(D^2-\alpha^2)^2}{i\alpha}\right\}\phi = 0, \tag{4}$$

$$\left\{\left[(V-c) - \frac{E(D^2-\alpha^2)}{i\alpha Pr}\right] \times \left[(V-c)(D^2-\alpha^2) - V'' - \frac{E(D^2-\alpha^2)^2}{i\alpha}\right] + Ri\right\}\phi = 0, \tag{5}$$

$$Ri = \frac{gS}{V_z^2},$$

$$D = \frac{d}{dz}.$$

The solution method for the sixth-order equation is discussed. The fourth-order solution is similar, while the second-order solution is relatively simple. The results are then used to discuss the validity, and practicality of using the lower order equations.

II. Solution of the Stratified Orr–Sommerfeld Equation

Governing Equation

$$\left[\frac{E(D^2 - \alpha^2)}{i\alpha Pr} - (V - c)\right] \times \left[\frac{E(D^2 - \alpha^2)^2}{i\alpha} - (V - c)(D^2 - \alpha^2) + V''\right] \phi + Ri\phi = 0 \qquad (6)$$

Boundary Conditions

Consider a solid wall maintaining constant temperature.

$$\begin{aligned} \phi(0) = \phi'(0) &= 0, \\ \overline{T}'(0) &= 0. \end{aligned} \qquad (7)$$

In terms of ϕ,

$$[(E(D^2 - \alpha^2)^2/i\alpha) - [V(0) - c](D^2 - \alpha^2) + V''(0)]\,\phi = 0$$

When the coefficients of the stratified O–S Eq. (6) vary in the range of interest, no closed form solution exists. However, a numerical integration is possible over the interval. Far from the boundary, where the velocity V_g and temperature $\overline{T}$ approach constant values, the O–S equation assumes the simple form

$$\phi^{vi} - (\lambda_1^2 + \lambda_2^2 + \lambda_3^2)\,\phi^{iv} + (\lambda_1^2\lambda_2^2 + \lambda_2^2\lambda_3^2 + \lambda_3^2\lambda_1^2)\,\phi'' - \lambda_1^2\lambda_2^2\lambda_3^2\phi = 0,$$

where

$$\begin{aligned} \lambda_1^2 &= \alpha^2 + (iPr/E)(V_g - c), \\ \lambda_2^2 &= \alpha^2 + (i\alpha/E)(V_g - c), \\ \lambda_3^2 &= \alpha^2. \end{aligned}$$

This differential equation of constant coefficients has six solutions expressible in terms of exponential functions

$$\begin{aligned} \phi_1 &= e^{-\lambda_1 y}, & \phi_2 &= e^{\lambda_1 y}, \\ \phi_3 &= e^{-\lambda_2 y}, & \phi_4 &= e^{\lambda_2 y}, \\ \phi_5 &= e^{-\lambda_3 y}, & \phi_6 &= e^{\lambda_3 y}. \end{aligned} \tag{8}$$

If the solutions are to remain bounded as $y \to \infty$, then ϕ_1, ϕ_3, and ϕ_5 are the only acceptable solutions. Since ϕ_1, ϕ_3, and ϕ_5 satisfy the O–S equation at the outer edge of the boundary layer, $y = y_0$, a general solution can be expressed as a combination of these three solutions. Anticipating a numerical integration of the O–S equation from the outer edge of the boundary layer to the wall, $y = 0$, ϕ_1, ϕ_3, and ϕ_5 (which are solutions to the simplified O–S equation) are used to specify initial values for numerical integration of the O–S equation. Using these initial values, Eq. (6) is integrated (the Runge–Kutta method is used here) to find the most general solution. Initially, the solutions are linearly independent. However, as the numerical integration proceeds, this linear independence is observed to disappear rapidly. The difficulty here is that a computer carries only a specified number of significant digits plus an exponent when representing a real number. Therefore, from time to time, a truncation or round off error $\pm\epsilon$ occurs. That is, at some integration step, say $(y - h)$, where h is the step size, we have

$$\phi(y - h) = c_1 \pm \epsilon. \tag{9}$$

At the next integration from $(y - h)$ to $(y - 2h)$, the truncation error $\pm\epsilon$ presents a suitable initial condition for obtaining the solution ϕ_3 and ϕ_5. Hence the solution obtained at the end of this step of the integration is the sum of the three solutions ϕ_1, ϕ_3, and ϕ_5, namely, $\phi(y - 2h) = \phi_1(y - 2h) \pm \epsilon\phi_3(y - 2h) \pm \epsilon\phi_5(y - 2h)$. This is because, at each integration step, the differential equation admits the more general solution based, e.g., on $\phi(y - h) = c_1 + c_2$ rather than the solution based on $\phi(y - h) = c_1$; in the present case $c_2 = \pm\epsilon$. Since ϕ_3 and ϕ_5 exhibit a much more rapid growth than does ϕ_1, the solution that started as ϕ_1 is dominated by the term $\pm\epsilon\phi_3 \pm \epsilon\phi_5$, if the integration proceeds far enough, and the linear independence of the three solutions is lost. The portion $\pm\epsilon\phi_3$ and $\pm\epsilon\phi_5$ of the solution ϕ_1 is commonly referred to as the parasitic error. Since the growth of ϕ_3 and ϕ_5 increases as E decreases, the contamination of the ϕ_1 solution is more pronounced at lower E (higher Reynolds number). Therefore numerical solutions are limited as E gets small.

Recently, Landahl and Kaplan [6] devised a purification scheme where, at each integration step, the slowly growing solution ϕ_1 is purified from its parasitic error $\pm\epsilon\phi_3$ and $\epsilon\phi_5$ such that at the end of the integration interval, ϕ_1 is not dominated by its parasitic error. The scheme was found successful in integrating

the O–S equation at Reynolds number ($Re = 1/E$) as high as 10 000. A different scheme based on a Gram–Schmidt orthagonalization has been suggested [7], and was found successful in obtaining solutions up to Reynolds number as high as 500 000.

In the present investigation, the Gram–Schmidt process is adopted [8]. At the end of a certain integration step, after using the Runge–Kutta integration procedure with a step of .01, proceeding downward from the outer edge boundary layer, we obtain a value for each of the three solutions ϕ_1, ϕ_3, and ϕ_5 and their derivatives. Next we carry out the Gram–Schmidt process leading to the new orthonormal solution vectors $\bar{\phi}(0.99)$, $\bar{\phi}_3(0.99)$ and $\bar{\phi}_5(0.99)$ where

$$\begin{aligned}
\bar{\phi}_5(0.99) &= \frac{\phi_5(0.99)}{|\,\phi_5(0.99)\,|}, \\
\bar{\phi}_3(0.99) &= \frac{\phi_3(0.99) - [\phi_3(0.99), \bar{\phi}_5(0.99)]\,\bar{\phi}_5(0.99)}{|\,\phi_3(0.99) - [\phi_3(0.99), \bar{\phi}_5(0.99)]\,\bar{\phi}_5(0.99)\,|}, \\
\bar{\phi}_1(0.99) &= \frac{\phi_1(0.99) - [\phi_1(0.99), \bar{\phi}_3(0.99)]\,\bar{\phi}_3(0.99) - [\phi_1(0.99), \bar{\phi}_5(0.99)]\,\bar{\phi}_5(0.99)}{|\,\phi_1(0.99) - [\phi_1(0.99), \bar{\phi}_3(0.99)]\,\bar{\phi}_3(0.99) - [\phi_1(0.99), \bar{\phi}_5(0.99)]\,\bar{\phi}_5(0.99)\,|},
\end{aligned} \tag{10}$$

where $[\phi_i, \phi_j]$ and $|\,\phi\,|$ represent the inner product and magnitude. By carrying out the same linear transformation on the initial vector

$$\phi_1(1.0) = \begin{bmatrix} 1 \\ -\alpha \\ \alpha^2 \\ -\alpha^3 \\ \alpha^4 \\ -\alpha^5 \end{bmatrix}, \qquad \phi_3(1.0) = \begin{bmatrix} 1 \\ -\beta \\ \beta^2 \\ -\beta^3 \\ \beta^4 \\ -\beta^5 \end{bmatrix}, \qquad \phi_5(1.0) = \begin{bmatrix} 1 \\ -\gamma \\ \gamma^2 \\ -\gamma^3 \\ \gamma^4 \\ -\gamma^5 \end{bmatrix},$$

we found the new initial vectors which lead to the three orthonormal vectors $\bar{\phi}_1$, $\bar{\phi}_3$, and $\bar{\phi}_5$. These initial conditions are

$$\bar{\phi}_5(1.0) = \frac{1}{|\,\phi_5(1.0)|} \begin{bmatrix} 1 \\ -\gamma \\ \gamma^2 \\ -\gamma^3 \\ \gamma^4 \\ -\gamma^5 \end{bmatrix},$$

$$\bar{\phi}_3(1.0) = \frac{1}{|\,\phi_3(1.0) - [\phi_3(1.0), \bar{\phi}_5(1.0)]\,\bar{\phi}_5\,|} \left[\begin{bmatrix} 1 \\ -\beta \\ \beta^2 \\ -\beta^3 \\ \beta^4 \\ -\beta^5 \end{bmatrix} - \frac{(\phi_3, \bar{\phi}_5)}{|\,\phi_5\,|} \begin{bmatrix} 1 \\ -\gamma \\ \gamma^2 \\ -\gamma^3 \\ \gamma^4 \\ -\gamma^5 \end{bmatrix} \right],$$

$$\bar{\phi}_1(1.0) = \frac{1}{|\,\phi_1 - (\phi_1\,,\,\bar{\phi}_3)\,\bar{\phi}_3 - (\phi_1\,,\,\bar{\phi}_5)\,\bar{\phi}_5\,|}$$

$$\times \left[\begin{bmatrix} 1 \\ -\alpha \\ \alpha^2 \\ -\alpha^3 \\ \alpha^4 \\ -\alpha^5 \end{bmatrix} - (\phi_1\,,\,\bar{\phi}_3)\,\bar{\phi}_3 - (\phi_1\,,\,\bar{\phi}_5)\,\bar{\phi}_5\right]. \tag{11}$$

We integrate the O–S equation from $y = 1.0$ to $y = 0.99$ using as initial conditions at $y = 1.0$ the solution $\bar{\phi}_1(1.0)$, $\bar{\phi}_3(1.0)$ and $\bar{\phi}_5(1.0)$. The vectors so obtained are orthonormalized and so are the conditions at $y = 1$. Continuing in this way, we eventually find three initial vectors which are initial conditions for the O–S equation leading to three orthonormal vectors at $y = 0$. In this way solutions of the O–S equation for which $\phi(\infty) \to 0$ are accurately determined.

III. Results

Second-Order Solutions

The singular nature of the second-order equation, obtained in the limit $E \to 0$ prevents investigation in the region where $V - c = 0$. However, since the behavior of the solutions near the maximum growth rate region is primarily of interest, calculations were made in the region of a maximum growth rate mode known from a higher order solution. For the second-order equation, since the eigenvalues have a real part phase speed nearly equal to V at the inflection point, $V'' = 0$, all of the terms are small, thereby increasing convergence problems.[1] Nevertheless, qualitative effects, such as consideration of a variable Ri with vertical coordinate z could be investigated. When a two-layer Ekman case was run, with $Ri = Ri_d$ at $z \leqslant z_c$, $Ri = Ri_u$ for $z > z_c$, the importance of Ri at the inflection point was evident, although the solutions were unstable near the critical height, $z_c \approx z_i$.

The instability mode in the vicinity of the maximum growth rate was well behaved and displayed a definite peak to be compared with a higher order solution [Fig. (2)]. The eigenfunction magnitude and phase for the stable case are shown in Fig. (3). Although the second-order equations yielded a single well-behaved instability region, the neutral stability curve and the location of the maximum growth rate did not correspond well to the higher order solutions.

[1] Although the second-order equation is not singular at $V = c_r$ if the growth rate is finite, i.e., $\alpha c_i \neq 0$.

In order to remove the uncertainties involved in a singular perturbation solution, and to avoid the numerical problems arising in separating the discrete spectrum from the continuous spectrum for the singular second-order equation, the viscous term must be included (E finite), producing a fourth-order equation at least.

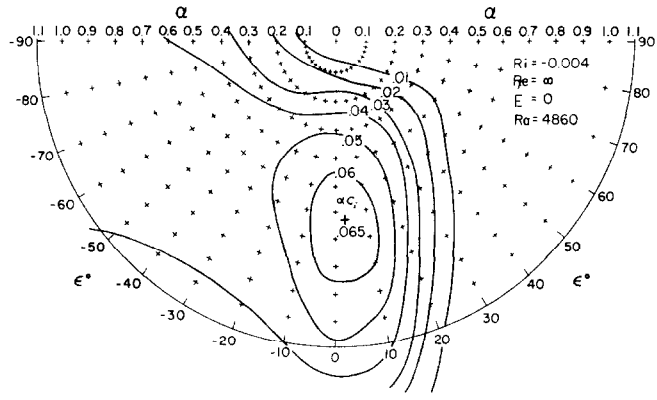

FIG. 2. Stability diagram showing growth rates αc_i in the vicinity of $\alpha c_{i\,\max}$ from the second order approximation. The two-dimensional perturbation is oriented $\epsilon + 90°$ to the left of the free-stream velocity. α and αc_i are nondimensionalized with respect to characteristic depth L and free-stream velocity V_a.

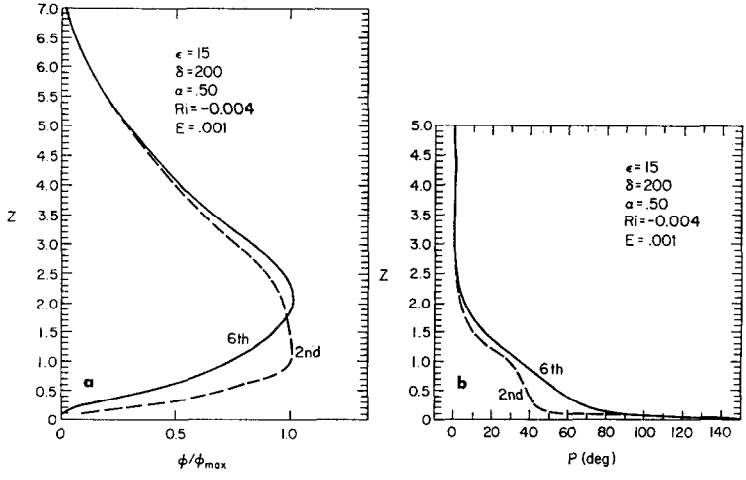

FIG. 3. (a) Typical eigenfunction solutions (vertical stream function shape) for near maximum growth rate conditions. The sixth-order solution is for small but finite E, the second-order solution is from $E \to 0$ limit equations. (b) The vertical phase distribution of the eigenfunction.

Fourth-Order Solutions

When the viscous terms are included, and the limits $Ri \to 0$, $Pr \to \infty$, considered, the fourth-order Orr–Sommerfeld equation is obtained. This equation is not singular, and admits neutral stability solutions. There is generally a single unstable mode, associated with the inflection point in the $V(z)$ profile. Once a particular eigenvalue for this mode has been found, the behavior of the solution as a function of the variable coefficients may be conveniently investigated using the shooting method. For the neutrally stratified fluid with an Ekman velocity profile, the unstable mode associated with the inflection point is the only unstable mode. The neutral stability curve for this mode is produced in Fig. (4). The fourth-order results were all reproduced by the sixth-order equations in the $Ri \to 0$ limit.

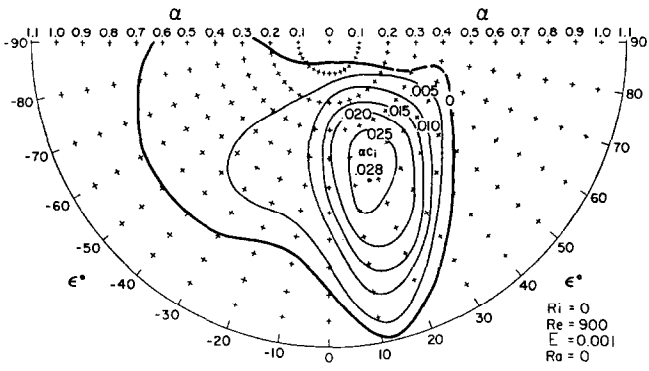

FIG. 4. Same as Fig. 2 except from the fourth-order solution for small E.

Sixth-Order Solutions

When the stratified fluid is considered, it is necessary to consider a sixth-order equation to avoid the singular second-order equation. There now exists the possibility of a convective (Rayleigh type) instability mode in addition to the dynamic mode. Since we are primarily interested in the inflection point mode, and the solution differences in the approximate equations, the effect of the additional parameter Ri upon this mode only was surveyed. The sixth-order solutions for variable $Ri(z)$ collaborate the second-order solutions, while yielding numerical solutions close to the critical layer due to the damping effect of the higher order terms. Figure 5, which shows the sixth-order results indicating the importance of Ri at the inflection point was also obtained from the second-order equations except the critical layer values were not damped and the magnitudes of c were different. Since the basic instability mechanism is of an inviscid nature, i.e., it is associated with the inflection point of the velocity profile, it was essentially independent of Pr or E for $E < .002$.

The sixth-order eigenvalues converge well to the fourth-order solution for $Ri \to 0$. The growth rates at a moderately unstable $Ri = -.004$ are shown in Fig. (6). The eigenvalue magnitudes and phase are given in Fig. (7a,b), for representative parameters. The eigenvalues and eigenfunctions are insensitive to small variations in E, α or ϵ relative to Ri variation.

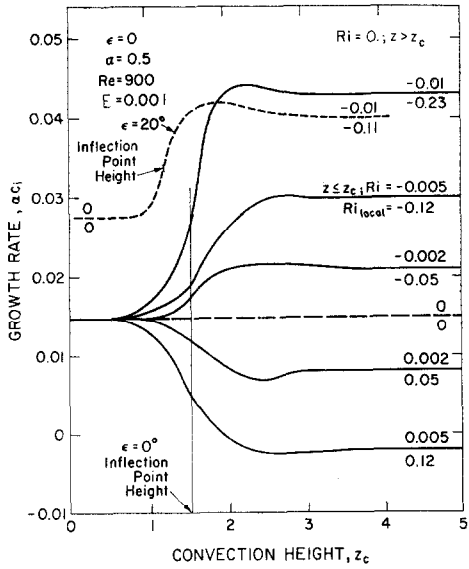

FIG. 5. Growth rates for two-step stratification, $Ri = 0, \pm 0.002, \pm 0.005, -0.01$ for $z \leqslant z_c$, $Ri = 0$ for $z > z_c$. Ri_{local} at the inflection point.

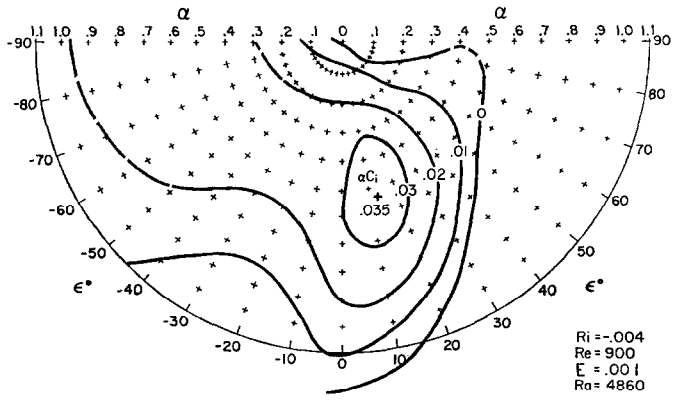

FIG. 6. Same as Fig. 2 except from the sixth-order solution for moderately instable stratification.

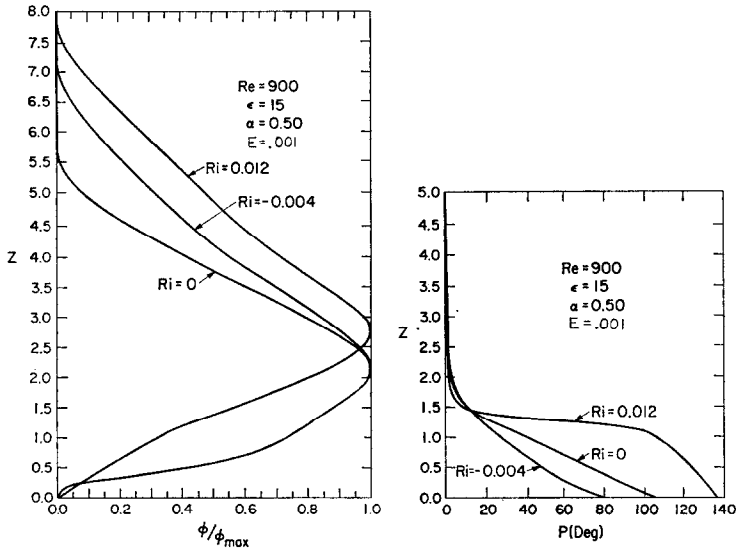

FIG. 7. (a, b) Same as Fig. 3, except sixth-order solutions for various stratifications.

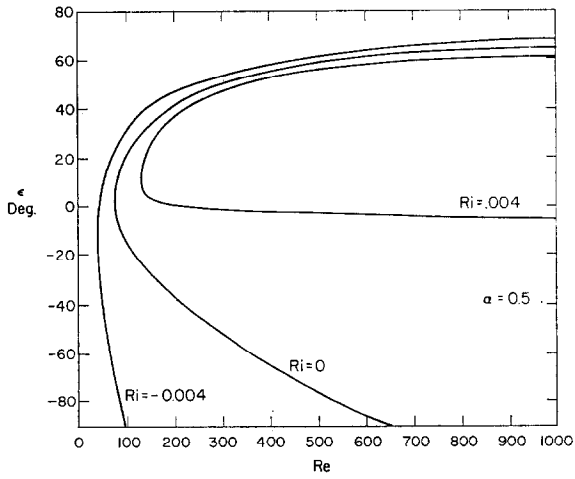

FIG. 8. Neutral stability curves for various stratifications as a function of orientation (ϵ) and $Re(1/E)$, inflection point instability.

The effect of stratification upon the neutral stability curve for ϵ *vs* Reynolds number (inverse of E) is shown in Fig. (8) for the rotating boundary layer profiles. The maximum growth rates occurred very close to $\alpha = .5$ in the range of ϵ, Ri and Re shown. The Coriolis term (requiring the eighth-order solution) can be

expected to become significant at very low $Re < 100$, further reducing Re minimum. The growth rates as a function of ϵ and Ri at supercritical E are shown in Fig. (9), with local Ri given by dashed lines. The variation of ϵ for maximum growth rate as a function of Ri is evident from this graph. Figure 10 shows the stratification effect on the Tollmein–Schlicting waves for a Blasius profile.

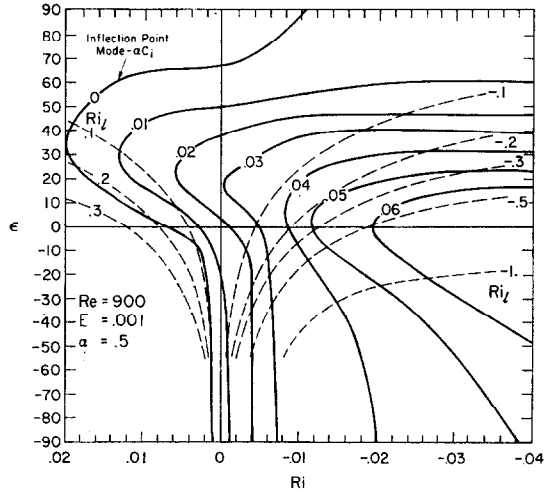

FIG. 9. Neutral stability and growth rate curves as a function of orientation (ϵ) and stratification (Ri). Ri_i is local value at the inflection point.

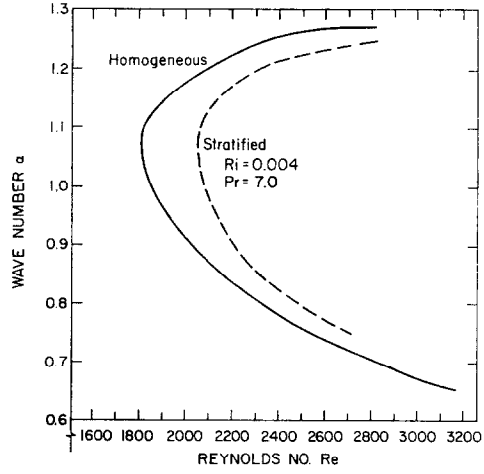

FIG. 10. Neutral stability curve shift for stable stratification of Tollmein–Schlicting viscous instability.

Considerable difficulty was encountered in obtaining the eigenfunction behavior accurately for certain ranges of the parameters. Although the average of the eigenfunction corresponded well to the smooth fourth and second-order solutions, the sixth-order eigenfunctions were generally irregular for wavenumbers greater than 0.4 and $E \leqslant .002$, and exhibited great sensitivity in the vicinity of the critical layer, where $V'' = 0$. When the step size was halved in the numerical calculation, no significant improvement was found.

The sixth-order solution was found to contain spurious unstable modes. Each eigenvalue mode was checked for dependence on step size in the integration, and appearance in the corresponding limit equation. Several apparent solutions were discarded on this basis as being computational in origin. One possible source of spurious modes is the generation of internal waves. A quick check of the corresponding Brunt–Vaisala frequency would identify this possibility.

IV. Discussion

The primary motivation for these solutions was to investigate the supercritical (with respect to E) behavior of the maximum growth rates for the inflection point instability mode of an Ekman velocity profile with respect to variation in the stratification parameter Ri. The principle conclusions involve the validity of the singular perturbation solutions obtained by letting $Ri \to 0$ and $Pr \to \infty$, reducing the sixth-order equation to the fourth order, and the limit $E \to 0$, yielding the second-order equation. The singular perturbation equation is generally faulted for "losing physical significance." This only means that it is not able to satisfy as many boundary conditions as the higher order parent equation, and will fail to yield a physically realistic solution to the extent that the boundary conditions are important. The present second-order equation has the complication of a singularity preventing solutions at eigenvalues approaching neutral stability, since the critical layer at $V = c_r$ must invariably be passed through in the integration.

A significant difficulty in obtaining the numerical solutions arises from using inadequate step sizes in the integration, leading to spurious solutions on the one hand, and completely masking the physically real solution on the other. A spurious mode may appear, smoothly varying with changes in the parameters, yet changing significantly with a variation in step size. In such a case, one may either continue decreasing step size until the solution doesn't change—with obvious practical limitations—or seek the source of the spurious mode, in the differencing method, the boundary conditions, or anomalous behavior with respect to a basic parameter. In some cases, the spurious mode can simply be ignored, if it doesn't interfere with the investigation of the physically real mode when the shooting method is

employed. Usually, the real mode can be identified through predicted behavior with respect to parameter variation obtained from asymptotic solutions. For instance, a mode which behaved much like a convective mode in other respects, did not vanish as the unstable stratification became zero, and was subsequently identified as associated with the implied inflection point at the upper boundary. In addition, a mode which was readily determined at low wavenumbers was not resolved in the residue/eigenvalue relationship when wavenumbers increased at constant step size. Thus, a varying step size is needed when surveying over large wavenumber ranges.

The shooting, or marching solution, allows direct tracing of one particular mode, thus minimizing the interference of the continuous spectrum solutions arising in the singular second order equation. Although the magnitude of the second-order eigenvalues differed significantly from those obtained in the higher order solutions, the mode was sufficiently close, and similarly behaved to be easily located with a nearby survey of boundary condition residues *vs* input eigenvalues. Away from the critical regions, the second-order solutions are qualitatively similar to the higher order solutions. The importance of Ri at the inflection point is clearly indicated by second-order solutions, although the solution deteriorates rapidly with increasing Ri. The eigenfunctions in the vicinity of the maximum growth rate are well behaved and representative of the higher order solutions (Figs. 3, 7). The second-order solutions possess a characteristic maximum in magnitude and phase change at low elevations ($z \leqslant 1.0$). This feature is damped and smoothed in the viscous solutions. The fourth-order solutions well represent the sixth-order solutions in the $Ri \to 0$, $Pr \to \infty$ limit confirming that this is not a singular perturbation limit.

The discrepency between critical values of α and ϵ for maximum growth rate between the second-order and the fourth- and sixth-order solutions apparently must be ascribed to the relative freedom allowed in the second-order solution. Due to the singular nature of the second-order equation, the results obtained from second order are reliable only for cases with sufficiently large growth rate. On the other hand, the accuracy of the higher order equations depends on the step size as well as the E number. The step size must be reduced as E decreases in order to orthonormalize the vectors with sufficient accuracy. Thus, although the higher order equations indicate independence of E for very small values, the lower order equation does not reproduce this solution. Hence, the solution is qualitatively an asymptotic solution, but there exist quantitative distortions due to the reduced number of boundary conditions satisfied by the second-order equation.

In all cases, the inner boundary conditions could be satisfied to almost arbitrarily small tolerances, 10^{-5} error usually being used. One of the main weaknesses of the shooting method is the difficulty in attaining convergence in the root finding scheme without accurate initial guesses for the eigenvalue. The use of the CDC's

Graphic Terminal greatly facilitated this process. The procedure used was to select three c_i values, a $c_{r_{min}}$ and a c_r increment. Then "shoot" an array of values, plotting the three resulting curves on a residue grid (Fig. 11). Visual interpolation

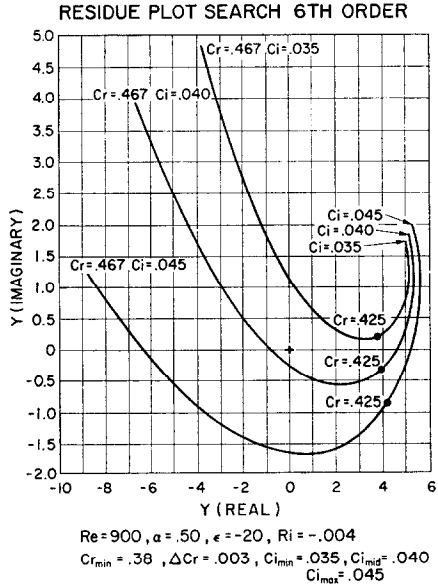

FIG. 11. Typical computer plot of boundary condition residue Y for array of 90 eigenvalues c. Interpolated eigenvalue to produce Aitkin process convergence, $c = (0.430; 0.039)$.

toward zero residue would be made until the automatic root finder (Aitkin method) could be used.

The following conclusions can be made based on the results:

(1) The $E \to 0$ limit equation exhibits singular behavior which greatly restricts any numerical surveys of the inflection point instability mode in the vicinity of the neutral stability curve and the critical layer ($V - c = 0$). In addition, although a mode which appears to be the asymptotic limit of the higher order solution appears, it has significantly different parameters for maximum growth rates, e.g., second-order $\alpha_c = .65$, $\epsilon_c = 5°$ whereas fourth- and sixth-order $\alpha_c = .5$, $\epsilon_c = 18°$.

(2) The addition of viscosity (finite E) removes the singular nature of the governing eigenvalue equation and quantitatively alters the solution. However, these solutions appear to be independent of E for $E < .002$. The step size dependence upon E limits $E \geqslant 10^{-4}$.

(3) The relative independence with respect to E of the fourth- and sixth-order solutions indicates that the small E condition can still be used to justify neglect of the Coriolis term—and hence the eight order equations—for $E < .002$.

(4) For investigation of a particular eigensolution with respect to variations of the problem parameters in the supercritical range of one of the parameters, the shooting method is more practical than the matrix method, which produces all of the eigenvalues each time. However, the shooting method is not well adapted to surveying for unknown eigenvalues. The best compromise is apparently an initial search using a matrix solution, switching to a shooting method for detailed modal behavior.

REFERENCES

1. A. P. GALLAGHER AND A. M. MERCER, On the behavior of small perturbations in plane Couette flow with a temperature gradient, *Proc. Roy. Soc. A* **286** (1965), 117–128.
2. T. ASAI, "Stability of a Plane Parallel Flow with Variable Vertical Shear and Unstable Stratification," NCAR Manuscript No. 69–194, National Center for Atmospheric Research, 1969.
3. D. K. LILLY, On the instability of Ekman boundary flow, *J. Atmos. Sci.* **23** (1966), 481–494.
4. R. A. BROWN, A secondary flow model of the planetary boundary layer, *J. Atmos. Sci.* **27** (1970), 742–757.
5. J. GARY AND R. HELGASON, A matrix method for ordinary differential eigenvalue problems, *J. Computational Phys.* **5** (1970), 169–187.
6. M. T. LANDAHL AND R. E. KAPLAN, The effect of compliant walls on boundary layer stability and transition, *Agardograph* **97** (1965), 353–373.
7. A. R. WAZZAN, T. OKAMARA AND A. M. O. SMITH, The stability of water flow over heated and cooled flat plates, *J. Heat Transfer Trans. ASME* (1968), 109–114.
8. R. COURANT AND D. HILBERT, "Methods of Mathematical Physics," Vol. I, p. 3, Interscience, New York, 1953.